Inorganic Chemistry

ARTICLE

pubs.acs.org/IC

Rare Examples of Fluoride-Based Multiferroic Materials in Mn-substituted $BaMgF_4$ Systems: Experimental and Theoretical Studies

Farheen N. Sayed,[†] B. P. Mandal,[†] O. D. Jayakumar,[†] A. Arya,[‡] R. M. Kadam,[§] A. Dixit,[⊥] R. Naik,[⊥] and A. K. Tyagi*[,†]

[†]Chemistry Division, [‡]Materials Science Division, [§]Radiochemistry Division Bhabha Atomic Research Centre Mumbai 400085, India

[⊥]Department of Physics and Astronomy, Wayne State University, Detroit 48201, Michigan, United States

Supporting Information

ABSTRACT: A series of Mn-substituted $BaMgF_4$ samples have been synthesized by a hydrothermal route. X-ray diffraction study reveals that the products are monophasic in nature. Scanning electron microscopy (SEM) and energy-dispersive spectrometry (EDS) studies were carried out to investigate the morphology and stoichiometry for these compounds. X-ray photoelectron spectroscoy (XPS) and electron spin resonance (ESR) studies were done to confirm the oxidation state of dopant ion. Room temperature ferromagnetism was observed on Mn substitution at the Mg site in $BaMgF_4$ samples. The saturation magnetization increases initially, shows a peaking effect, and then decreases with further increase in Mn concentration in $BaMg_{1-x}Mn_xF_4$ ($0.0 \le x \le 0.15$). However, ferroelectricity was found to decrease with an increase in Mn concentration in the series of investigated $BaMg_{1-x}Mn_xF_4$ ($0.0 \le x \le 0.15$) samples. First-principle calculations, using the projector augmented wave potentials on Mn-substituted $BaMgF_4$, confirmed the decrease in magnetic moment with an increase in Mn content beyond certain concentration. These samples exhibit very weak magnetocapacitive coupling, which can be attributed to the very small magnetic signal observed in these samples.

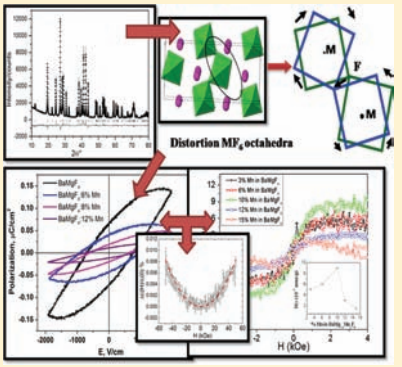

1. INTRODUCTION

Multiferroics represent a unique class of magnetoelectric materials where ferro/antiferromagnetic and ferro/antiferroelectric properties coexist simultaneously exhibiting electromagnetic coupling.[1−3] However, a large number of multiferroic materials having ferroelectric (FE) and antiferromagnetic (AFM) ordering whereas only a very few multiferroics having simultaneously ferroelectric and ferromagnetic (FM) properties[4−6] are reported. Such materials are being contemplated for applications in memory, read−write electronic devices. In view of their immense potential, extensive research is being carried out on nano or bulk, thin film, and single crystal geometries of these materials.[7,8] Several perovskite materials such as $BiFeO_3$, $BiMnO_3$, $HoMnO_3$, $YMnO_3$, and $TbMnO_3$ have been reported as multiferroic materials.[9−12] It is worth mentioning that compared to oxides, there are not many fluoride-based ferroelectric materials, as fluorides usually adopt high symmetry (centrosymmetric space group) which does not support the ferroelectricity. To the best of our knowledge, there is no fluoride based material with the coexistence of ferroelectricity and room temperature ferromagnetism (RTFM).

$BaMgF_4$ is known to be a ferroelectric and diamagnetic material. In order to induce ferromagnetism in this material, Mn was chosen as a dopant, which has been reported to induce room temperature ferromagnetism (RTFM) in ZnO and In_2O_3 etc.[13,14] $BaMgF_4$ crystallizes with the polar space group[15] $Cmc2_1$. In this base-centered orthorhombic structure, the Mg^{2+} cations are octahedrally surrounded by fluoride anions. Four of the six corners of the MgF_6 octahedra are shared with adjacent MgF_6 octahedra to form puckered sheets perpendicular to the *b*-axis. These octahedra are separated by Ba cations which form BaF_8 polyhedra. Since Mn^{2+} is an isovalent ion to Mg^{2+} and sizewise also Mn^{2+} ion (0.83 Å in octahedral coordination) is comparable to Mg^{2+} (0.72 Å in octahedral coordination) ion,[16] it was considered as an ideal choice for substitution to introduce RTFM in $BaMgF_4$.

It is very important to mention here that several authors have written articles emphasizing the tendency in obtaining P-E (polarization-electric field) data which may be an artifact of ferroelectricity.[17−23] In a lucid article, Scott has suggested that the materials which show saturation in polarization and have a concave region in their P-E plot are true ferroelectrics.[17]

2. EXPERIMENTAL SECTION

The starting materials for the synthesis of undoped and Mn-doped $BaMgF_4$ were analytical grade $Ba(NO_3)_2 \cdot 4H_2O$ (purity 99.99%), $Mg(NO_3)_2 \cdot 6H_2O$ (purity 99.99%), $Mn(NO_3)_2 \cdot 4H_2O$ (purity 99.99%), and NH_4HF_2. In order to synthesize pure $BaMgF_4$, 0.2613 g of $Ba(NO_3)_2$, 0.3840 g of $Mg(NO_3)_2$, and 0.5130 g of NH_4HF_2 were added in 15 mL of deionized water. The reaction mixture was transferred

Received: August 23, 2011
Published: October 20, 2011

Table 1. Phase Analysis under Different Reaction Conditions

mole ratio						
$Ba(NO_3)_2 \cdot 4H_2O$	$Mg(NO_3)_2$	NH_4HF_2	pH	temp (°C)	duration (h)	phase information
1	1	9	5.5	120	36	$BaMgF_4 + BaF_2$
1	1.1	9	5.5	120	24	$BaMgF_4 + BaF_2$
1	1.4	9	5	120	60	$BaMgF_4 + BaF_2$
1	1.4	9	4	120	60	$BaMgF_4 + BaF_2$
1	1.4	8	4	150	60	$BaMgF_4 + BaF_2$
1	1.5	9	4	160	60	$BaMgF_4$
1	1.5	9.5	4	150	60	$BaMgF_4$

to a Teflon-lined stainless-steel autoclave and sealed and heated at different temperatures for different duration. Subsequently the autoclave was cooled, and the residue obtained was washed thoroughly with deionized water, followed by ethanol and then dried in air. The ratio of the starting materials, pH, reaction time, and temperature were found to be very crucial for the formation and crystallization of mono phasic products. After standardization of the synthetic procedure for pure $BaMgF_4$, several Mn-doped compositions were also synthesized with general composition $BaMg_{1-x}Mn_xF_4$ ($0.0 \le x \le 0.15$).

In order to determine the phase purity, powder X-ray diffraction data were recorded on a PANalytical X'pert Pro X-ray Diffraction (XRD) unit with monochromatized Cu−Kα radiation. The diffraction patterns were recorded in a step scan mode with step width 0.02° and step time 3.30 s. The morphological and compositional characterizations of these samples were carried out using a JEOL JSM840 scanning electron microscope (SEM) attached with energy dispersive spectrometry (EDS) facility. In order to determine the oxidation state of Mn in these compositions X-ray photoelectron spectroscopy (XPS) studies has been performed using Al Kα X-ray source (PHI model 550 ESCA/Sam system). It has been again confirmed by electron paramagnetic resonance (EPR) measurement. The EPR spectra were recorded on a Bruker ESP-300 spectrometer operating at X-band frequency (9.5 GHz) equipped with 100 kHz field modulation and phase sensitive detection to obtain a first derivative signal. Diphenyl picrylhydrazyl (DPPH) was used for calibration of the *g*-values of paramagnetic species. DC magnetization measurements, as a function of field, were carried out using an E.G. and G P.A.R vibrating sample magnetometer (model 4500) and the electrical polarization was measured on the thin pellets by a homemade LCR circuit. The pellets of the samples were made using an isostatic press and sintered at 500 °C for 4 h in argon atmosphere.

3. RESULTS AND DISCUSSION

3.1. Synthesis. The ratio of reactants, pH, temperature, duration, resulting phases, etc. are summarized in Table 1. It has been found that these parameters, in particular ratio of the reactants and duration of autoclaving, were found to be very crucial for the formation and crystallization of monophasic products in this system. In the synthesis of these compounds, NH_4HF_2 has several functions, as it acts as fluorinating agent, it helps to maintain the pH of the solution, and F^- ions are effective mineralizers. The excess of F^- ions helps in decreasing the reaction time and crystallization temperature.[24,25] The Mg/Ba ratio is a decisive factor for the formation of pure $BaMgF_4$. When the concentration of $Mg(NO_3)_2$ is less than 1.5 times of that of $Ba(NO_3)_2$, a biphasic mixture of $BaMgF_4$ and BaF_2 has always been obtained, irrespective of reaction temperature and time. The presence of excess BaF_2 as an impurity phase during the formation of $BaMgF_4$ suggests that sufficient

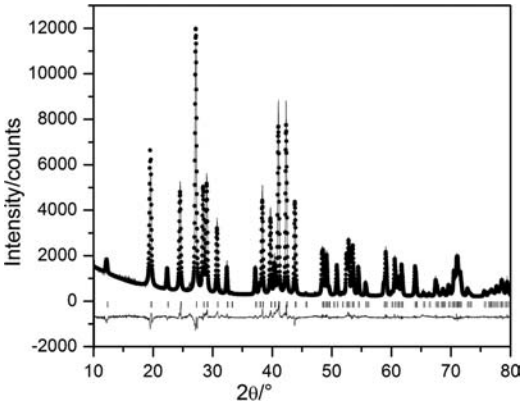

Figure 1. Rietveld refined XRD pattern of the $BaMgF_4$.

amount of Mg source was not present in the solution. In order to compensate for the deficiency of Mg source, Mg/Ba ratio in the solution was increased. Another interesting observation was that the excess NH_4HF_2 facilitates the formation of monophasic products. As mentioned earlier, pH also plays an important role in the formation of pure $BaMgF_4$ (see Table 1). Zhao et al.[24] also found that pH plays a crucial role during the synthesis of complex fluorides like $LiYF_4$, KYF_4, etc. In order to synthesize complex fluorides often HF is used which is chemically hazardous due to its corrosive nature. In the present synthesis procedure, NH_4HF_2, which is safe to handle, has been used instead of highly corrosive HF.

Once the molar ratio of $Ba(NO_3)_2$, $Mg(NO_3)_2$, and NH_4HF_2 was fixed for formation of single phasic product at 150 °C, a series of experiments were performed to follow the mechanism of the formation of $BaMgF_4$.

The products were collected at different times of autoclaving, and it has been found that initially BaF_2 and MgF_2 form after addition of NH_4HF_2 in the solution. After 30 h of reaction, the products were analyzed and were found to be a mixture of $BaMgF_4$ and BaF_2, which implies that the excess Mg^{2+} ions remained in solution and did not get precipitated. It has been found that content of BaF_2 decreases with increase in reaction time and that of $BaMgF_4$ increases because the unreacted BaF_2 reacts with MgF_2, present in the solution, and gives rise to pure $BaMgF_4$. Initially, the seeds of $BaMgF_4$ form, and then, MgF_2 in solution phase start to react with precipitated BaF_2. The other compositions in the series were synthesized with different Mg and Mn mole ratios.

3.2. Characterization. The XRD patterns of all the products in the $BaMg_{1-x}Mn_xF_4$ ($0.0 \le x \le 0.15$) series were recorded and

dx.doi.org/10.1021/ic201835q |*Inorg. Chem.* 2011, 50, 11765–11772

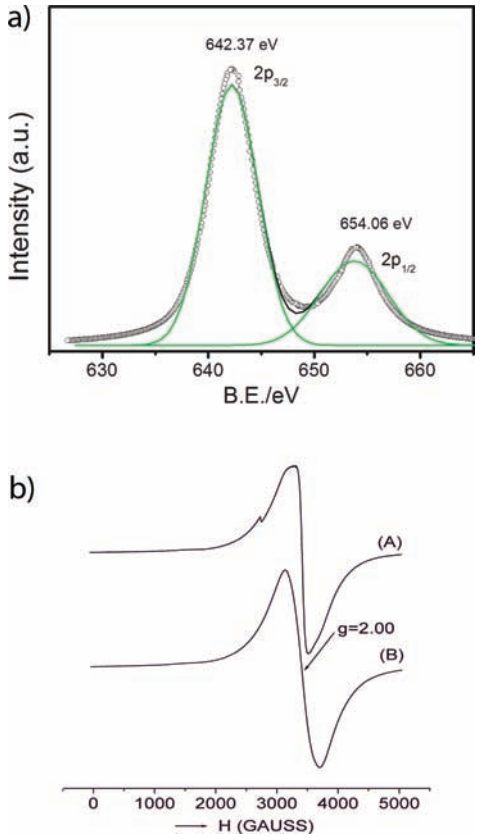

Figure 2. (a) XPS spectra of 12 at % Mn doped $BaMgF_4$ sample. (b) X-band EPR spectra of (A) $BaMg_{0.94}Mn_{0.06}F_4$ and (B) $BaMg_{0.88}Mn_{0.12}F_4$ at room temperature.

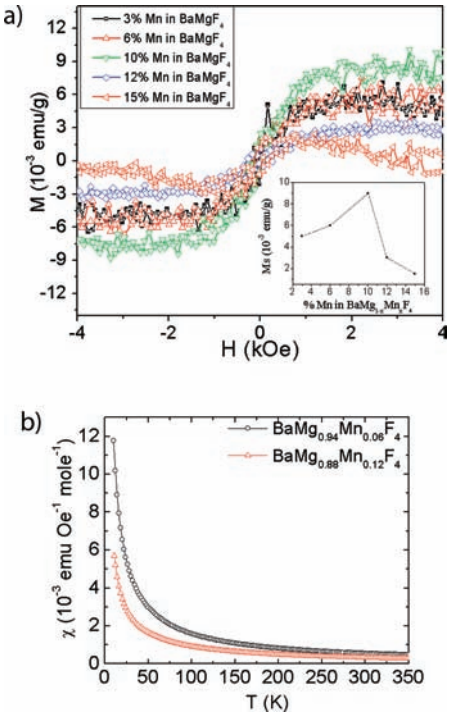

Figure 3. (a) Ferromagnetic M−H hysteresis curve. (inset) Variation of saturation magnetization with composition. (b) Variation of magnetic susceptibility with temperature in $BaMg_{1-x}Mn_xF_4$ series.

analyzed (Supporting Information 1). The XRD pattern of the parent compound $BaMgF_4$ was refined (Figure 1) using the Rietveld refinement with FullProf-2005 software. The obtained cell parameters for $BaMgF_4$ are $a = 4.131(1)$ Å, $b = 14.511(2)$ Å, $c = 5.816(2)$ Å, and volume = 348.6(4) Å^3 (R_p 8.3%, R_B-factor 9.5%). The refined position coordinates and unit cell parameters are close to the values reported in literature for $BaMgF_4$.[26] The cell volume of $BaMg_{1-x}Mn_xF_4$ compositions gradually increases from 346.6(3) to 352.3(3) Å^3 on increasing the Mn content from 0 to 15 at %, which can be explained on the basis of relative ionic radii of Mn^{2+} and Mg^{2+} (0.83 and 0.72 Å, respectively, in octahedral coordination).[16] It can be inferred from this observation that Mn^{2+} is getting incorporated at the Mg site into the lattice of $BaMgF_4$.

The morphological and compositional characterizations of these samples were carried out using SEM attached with EDS facility. Most of the grains were found to be regular with rectangular and hexagonal shapes (Supporting Information 2), which is a common observation for samples synthesized under mild hydrothermal conditions. The ratios of Ba:Mg:Mn in different compositions as per EDS data are shown in Supporting Information 3.

In order to determine the oxidation state of Mn in this series ($BaMg_{1-x}Mn_xF_4$ ($0.0 \le x \le 0.15$)), XPS has been carried out. In 12 at % Mn doped $BaMgF_4$ sample, XPS peaks have found at 642.37 and 654.06 eV which correspond to Mn $2p_{3/2}$ and $2p_{1/2}$ peaks (Figure 2a). Aoki[27] and Carver et al.[28] reported that Mn $2p_{3/2}$ peak in MnF_2 appears at 642.2 eV which confirms that in titled compounds also Mn is in +2 oxidation state. Moreover, the nature of the peak is symmetric which implies that no other Mn ions are present in the sample. Figure 2b shows the X-band EPR spectra of $BaMg_{0.94}Mn_{0.06}F_4$ and $BaMg_{0.88}Mn_{0.12}F_4$ at room temperature. In both cases, EPR spectra consisted of broad signal at g ca. 2.00 without any hyperfine and superhyperfine structure. The line widths were found to be 260 and 580 G for sample $BaMg_{0.94}Mn_{0.06}F_4$ and $BaMg_{0.88}Mn_{0.12}F_4$, respectively. The absence of hyperfine structure (^{55}Mn, $I = 5/2$, 100% abundance) and superhyperfine structure (^{19}F, $I = 1/2$, 100% abundance) in the EPR spectra of both these samples is because of the increased line width caused by dipole−dipole interaction. It is expected that the Mn^{2+} ions ($r = 0.83$ Å) substitute for Mg^{2+} ions ($r = 0.72$ Å), not Ba^{2+} ions ($r = 1.61$ Å) in $BaMgF_4$ because of the ionic radius of Mn^{2+} is considerably smaller than that of Ba^{2+} and also there is the isomorphous compound $BaMnF_4$. This observation is in conformity with the changes in the lattice parameter of undoped and Mn doped compounds. It may be argued that the presence of strong long-range interaction between the distant Mn^{2+} spins is responsible for the observed multiferroic properties or the formation of an impurity $BaMnF_4$ phase at higher doping concentrations of Mn is contributing for this effect. However, the later possibility is ruled out as $BaMnF_4$ is reported to undergo paramagnetic to antiferromagnetic transition at very low temperature ($T_N = 25$ K).

3.3. Magnetic Properties. The magnetic field dependent magnetization data for $BaMg_{1-x}Mn_xF_4$ for $x = 0.03$, 0.06, 0.10, 0.12, and 0.15 samples, at room temperature, are shown in Figure 3a, where paramagnetic contribution was subtracted to extract the effective ferromagnetic contribution for all samples. The pristine $BaMgF_4$ sample did not show any ferromagnetism, whereas the onset of room temperature ferromagnetism was observed for samples with a sufficient fraction of Mn ion at Mg sites. There is a systematic increase in saturation magnetization,

dx.doi.org/10.1021/ic201835q |Inorg. Chem. 2011, 50, 11765–11772

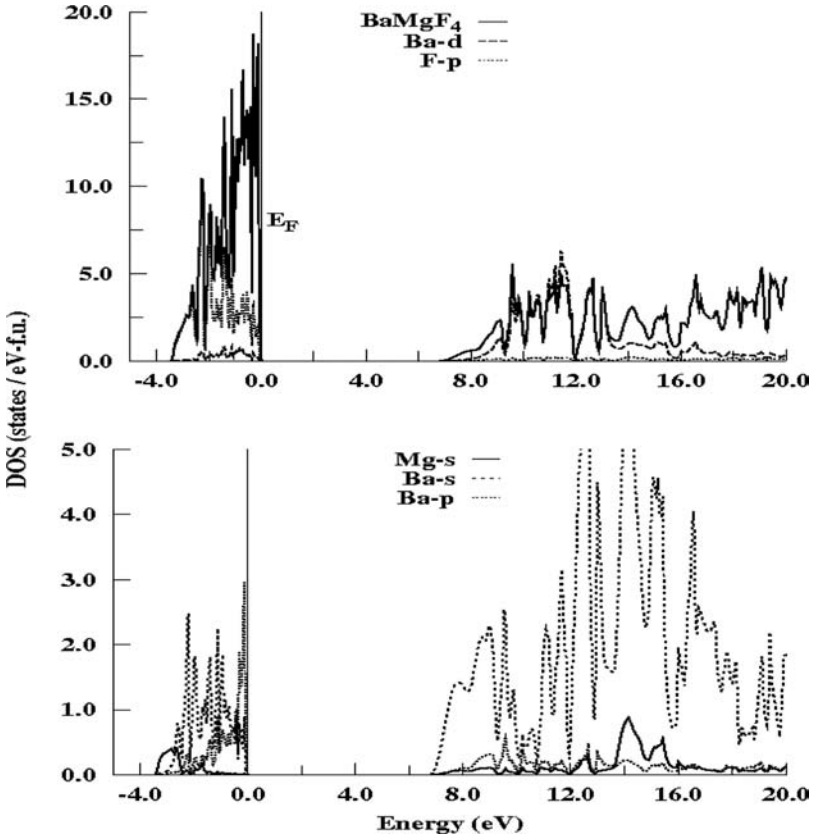

Figure 4. Total and site- and *l*-projected partial DOS for pure $BaMgF_4$. The spin components of DOS have been added together to show the total (spin-neutral) DOS. The abbreviation f.u. stands for formula unit.

and it is maximum for the $x = 0.10$ sample. At higher values of x, a decrease in saturation magnetization was observed, as shown in inset in Figure 3a. This is in agreement with theoretical calculations, discussed later. Thus, a critical concentration of Mn fraction is very important for the optimized room temperature ferromagnetic properties in $BaMg_{1-x}Mn_xF_4$ ($0.0 \leq x \leq 0.15$) compounds. The observed magnetism can be explained by ferromagnetic coupling between Mn^{2+} ions until a critical concentration, and above this critical concentration, possibly antiferromagnetic coupling starts playing important role due to decreased distance between them. The representative temperature dependence of magnetic susceptibility for 6 and 12 at % Mn doped $BaMgF_4$ samples are shown in Figure 3b. At low temperature, the paramagnetic Curie−Weiss behavior leads to a larger susceptibility, common behavior for week ferromagnetic systems.[29,30] We do not notice any signature of ferromagnetic transition up to 350 K, suggesting much higher ferromagnetic transition temperature for these $BaMg_{1-x}Mn_xF_4$ ($0.0 \leq x \leq 0.15$) samples.

3.4. Theoretical Interpretation. In order to understand the origin of magnetic behavior in these samples first principle calculations were performed on selected samples and have been described in next section.

We performed projector augmented wave (PAW) potential spin-polarized plane-wave-based DFT calculations on $BaMgF_4$ (Sp. Gr. = $Cmc2_1$), $BaMg_{0.875}Mn_{0.125}F_4$ (SC1), and $BaMg_{0.8125}Mn_{0.1875}F_4$ (SC2) using the generalized gradient approximations (GGA) for the exchange-correlation potential, as parametrized by Perdew−Burke−Ernzerhof.[31] We used the "Vienna ab initio simulation package" (VASP), which solves the Kohn−Sham equations using a plane wave expansion for the valence electron density and wave functions.[32] The interactions between the ions and electrons are described by the projector augmented wave (PAW) potentials, which use smaller radial cutoffs (core radii) and reconstruct the exact valence wave function with all nodes in the core region.[31] The PAW potentials used in this study are those provided in the VASP database (version 4.6). For Ba, we treated $5s^25p^66s^2$; for Mg, $3s^23p^0$; for F, $2s^22p^5$; and for Mn, $3p^64s^23d^5$ states as valence states. Our calculations are fully converged with respect to size of the basis set (kinetic energy cutoff, E_cutoff = 400 eV) and the number of **k**-points in the irreducible Brillouin zone (IBZ = 50 and 36 for both SC1 and SC2). The Mn-doped supercells (SC1 and SC2) were created by generating a primitive $2 \times 1 \times 2$ cell of $BaMgF_4$ unit cell. Each of these supercells contained 96 atoms of which 16 atoms were, originally, Mg equally distributed in eight sublatices. The substitution of 2(3) Mg atoms out of these 16 Mg sites led to 16(12) possible configurations for SC1 (SC2). This reduced further to only 6(4) distinct configurations on application of symmetry. Our calculations predicated the total energies of these 6(4) configurations to differ by not more than 20 meV/atom. For the sake of brevity, we present here the results for the most stable configuration of SC1 (SC2) unit cell with dopant percentage restricted to 12.50 at % (18.75 at%).

The equilibrium volume of $BaMgF_4$ was calculated to be 351.88 $Å^3$ ($a = 4.137$ Å, $b = 14.582$ Å, $c = 5.833$ Å) in very good agreement with experimental value. The equilibrium volumes of SC1 and SC2 (normalized with that of $BaMgF_4$) are 352.23 and 353.51 $Å^3$, respectively. The calculated ground state cohesive energies of $BaMgF_4$, SC1, and SC2 were −4.754, −5.598,

dx.doi.org/10.1021/ic201835q |*Inorg. Chem.* 2011, 50, 11765–11772

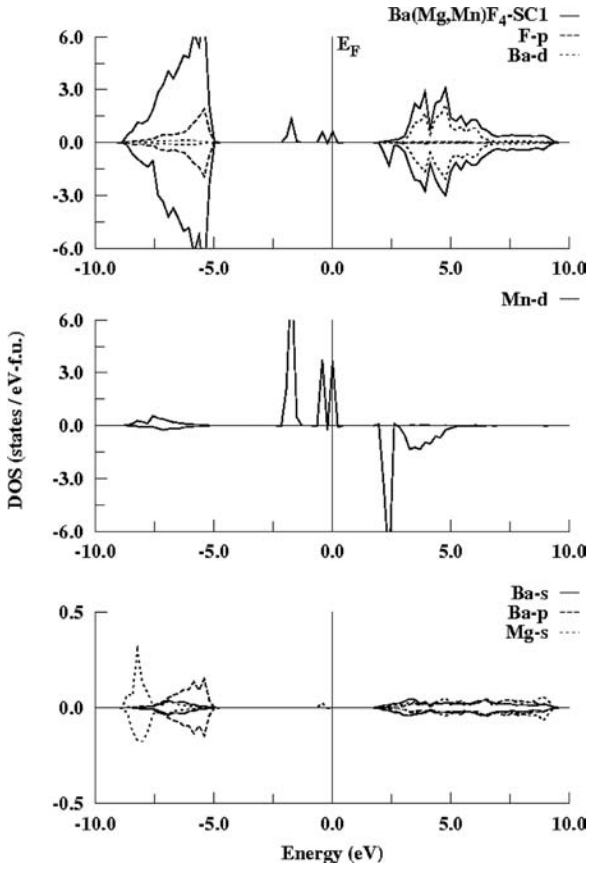

Figure 5. Total and site- and *l*-projected partial spin-polarized DOS for the $BaMg_{0.875}Mn_{0.125}F_4$ (SC1) supercell.

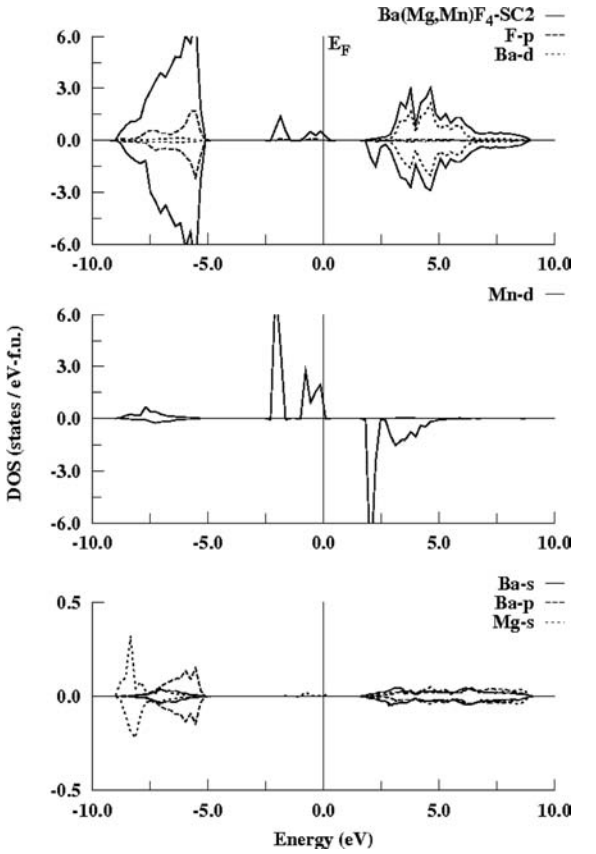

Figure 6. Total and site- and *l*-projected partial spin-polarized DOS for the $BaMg_{0.8125}Mn_{0.1875}F_4$ (SC2) supercell.

and −5.633 eV/atom, respectively, which show that the addition of Mn makes $BaMgF_4$ more stable and stability increases with increase in Mn content. Our spin-polarized calculations gave the net magnetic moment of $BaMgF_4$, SC1, and SC2 as 0.000, 5.000, 4.674 μ_B/Mn atom, respectively, in agreement with the finding that increase in Mn concentration brings down the ferromagnetism in $Ba(Mg,Mn)F_4$.

Figure 4 shows total and site- and *l*-projected partial density of states (DOS) for pure $BaMgF_4$. Since it does not exhibit any net magnetic moment, the spin components of DOS have been added together to show the total (spin-neutral) DOS.

The valence band, having the mixing of F-p, Mg-s, and Ba-p states in the total DOS plot, is fully occupied and exhibits a band gap with the conduction band, which mainly consists of Ba-s,d and Mg-s states. The calculated band gap is about 6.64 eV which is overestimated in comparison to the experimentally observed band gap of 5.63 eV (Supporting Information 4). The calculated band gap should be considered as the upper bound to the actual band gap as it is always overestimated in DFT-(LDA,GGA) calculations. The effect of Mn substitution can be seen in Figures 5 and 6, where we have plotted total and site- and *l*-projected partial spin-polarized DOS for SC1 and SC2, respectively. The valence band, now, mainly is composed of up-spin component of Mn-d with a slight contribution coming from up-spin component of Ba-p states. The valence and conduction bands in pure $BaMgF_4$ have been pushed toward the higher binding energy in both SC1 and SC2, maintaining the same gap. The difference between the up-spin and down-spin DOS, mainly for Mn-d states, is quite evident in Figures 5 and 6 and is responsible for high net magnetic moment for both SC1 and SC2 compounds. The up-spin component of DOS is partially unoccupied; while the down-spin component belongs to the conduction band. For SC1, the up-spin DOS at the Fermi level is quite high (Figure 5) as compared to that for SC2 (Figure 6). The valence band in SC1 exhibits stronger peaks (and hence stronger interactions among states) as compared to that in SC2, which may be responsible for higher magnetic moment in the former.

3.5. Electrical Properties. The ferroelectric (P-E) hysteresis loops of these compositions at room temperature are shown in Figure 7a. The characterization of ferroelectric materials from P-E loop is indeed crucial and often leads to misleading conclusions. It has been earlier reported that the materials which show saturation in polarization and have concave region in P-E plot are true ferroelectric.[16] In this investigation also the samples showed saturation polarization and concave region, thereby indicating the presence of intrinsic ferroelectricity in these samples. The area of the hysteresis loop of pure $BaMgF_4$ is larger than that of the doped samples. The electrical saturation polarization (P_s) and coercive field (E_c), obtained from the PE hysteresis loops, as a function of Mn^{2+} concentration are shown in Figure 7b. It was found that the variation of electrical saturation polarization (P_s) and coercive field (E_c) is opposite as a function of Mn^{2+} concentration in $BaMgF_4$. The sample with 6 at % Mn^{2+} substitution was found to have the highest coercivity, but its remnant polarization was low. It may be noted that $BaMgF_4$ does not contain any ions which are generally considered to be "ferroelectrically active" like d^0 cations or lone pair-active cations such as Bi^{3+} or Pb^{2+}. Also, there is no

dx.doi.org/10.1021/ic201835q |*Inorg. Chem.* 2011, 50, 11765–11772

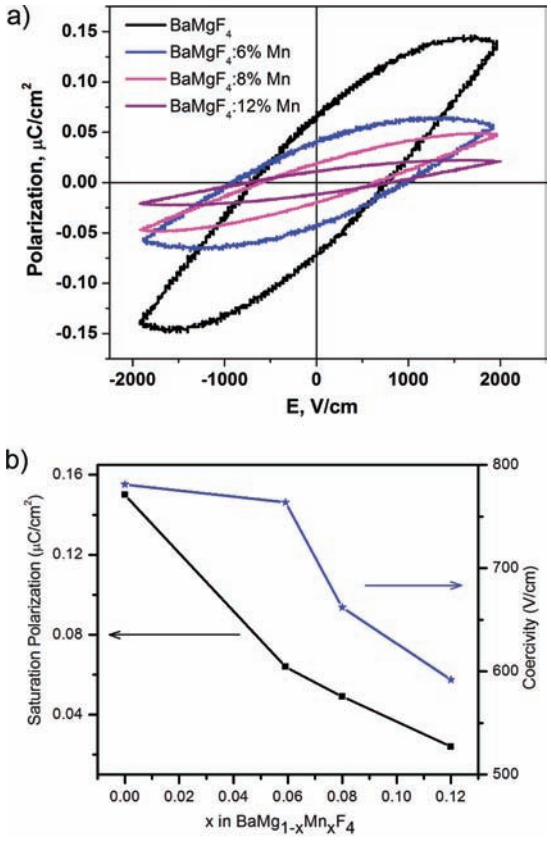

Figure 7. (a) Ferroelectric (P-E) hysteresis loops of different samples. (b) Electrical saturation polarization and coercivity as a function of Mn concentration in $BaMg_{1-x}Mn_xF_4$ series (measured at 100 Hz).

charge transfer between anions and cations in $BaMgF_4$ like that in $BiFeO_3$ or $BiMnO_3$. The ferroelectricity in $BaMgF_4$ is solely due to geometrical distortion. In these compositions, the ferroelectricity originates due to the softening of a single polar phonon mode, which involves both rotational motions of the MF_6 octahedra and displacements of the Ba cations caused due to relative ionic size effects and geometrical constraints.[32] It can be mentioned here that the crystal structure of $BaMgF_4$ consists of stacks of the puckered sheets formed by corner connected MgF_6 octahedra and BaF_8 along the *b*-axis (Figure 8). The origin of ferroelectricity in this class of material are related to the distortion of polyhedra.[34] In ref 33, it has been suggested that variation of M cation of $BaMF_4$ are reflected in distortion and hence on the ferroelectricity. In this study we also observe a possible sequential variation in distortion parameter with substitution of Mn in place of Mg. The distortion of $BaMgF_4$ is calculated from the observed data while for that comparing that of $BaMnF_4$ is calculated from the literature data. The distortion has been calculated using the formula. The distortion parameters have been calculated by following equation.

$$\Delta = 1/6\Sigma\{(d_i - \langle d\rangle)/\langle d\rangle\}^2$$

The bond length used for calculations of distortion parameter are given in Table 2. The MgF_6 octahedra are distorted significantly, and the Mg−F−Mg angles show appreciable deviation from the linear configuration (180°).[34,35] Typical Mg−F−Mg bond angles in the $BaMgF_4$ are 150.7 and 174.0°. In comparison, the analogous Mn−F−Mn bond angles in the isostructural $BaMnF_4$

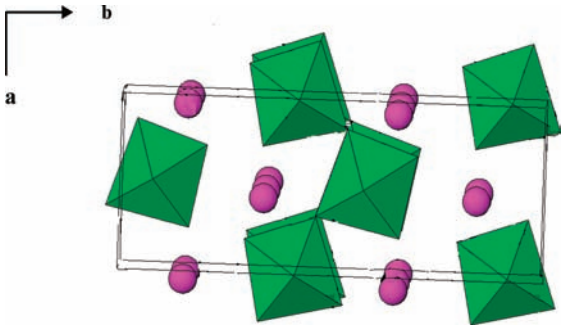

Figure 8. Unit cells of $BaMgF_4$. Green octahedra indicate the MF_6 unit, and pink spheres are Ba atoms. These octahedra are not connected linearly. the greater the deviation from 180°, the greater the distortion. With an increase in size of the M ion, the distortion decreases and the ferroelectricity decreases.

Table 2. Bond Lengths (Å) for Calculations of Distortion Parameter

Mg−F	1.934	1.948	1.980	2.015	2.066 × 2
Mn−F	2.037	2.042	2.115 × 2	2.129	2.151
BaF_8 (in Mn)	2.588	2.666 × 2	2.704 × 2	2.871	2.880 × 2
BaF_8 (in Mg)	2.604 × 2	2.633	2.675 × 2	2.845	2.880 × 2

are 138.7 and 173.0°. Also, it is observed[35] that the distortion parameter in the MgF_6 octahedra in $BaMgF_4$ is 6.8×10^{-4} while that of the MnF_6 in the $BaMnF_4$ is 4.1×10^{-4}. Thus it is easy to comprehend that there will be a decreasing trend in the distortion of MgF_6 octahedra on the incorporation of Mn^{2+} in the $BaMgF_4$ lattice. Similarly, the distortion parameter of BaF_8 polyhedra in the $BaMgF_4$ and $BaMnF_4$ lattices also show a decreasing trend (25.5×10^{-4} and 24.5×10^{-4}, respectively). The origin of ferroelectricity in $BaMgF_4$ type structure has been explained predominately from the displacement of Ba^{2+} ions compared to the F^- ions.[35] Recently, Ederer et al.[34] have shown theoretically that the cation and anion displacements in $BaMF_4$ structure decreases with the decrease in ionic radii of the M^{2+} ion. Also it has been pointed out that the energy gap between the ferroelectric and paraelectric state of the $BaMF_4$ structure significantly decreases with the decrease in ionic radii indicating a lowering trend of polarization. However, in contrast to these reported theoretical data, an opposite trend in the polarization with ionic radii is observed in the present study on $BaMg_{1-x}Mn_xF_4$ ($0.0 \le x \le 0.15$) compositions. The average M^{2+} cationic size increases in $BaMg_{1-x}Mn_xF_4$ ($0.0 \le x \le 0.15$) and the size of ferroelectric loop area decreases. It may be further added that the addition of the Mn^{2+} ion in the $BaMgF_4$ is expected to decrease the distortion in BaF_8 polyhedra.[35] Owing to the decreased distortion in the BaF_8 and MF_6 units, the off-centric displacement is likely to be decreased with the incorporation of Mn^{2+} ions, which is in excellent agreement with the experimental P-E data of this study. Earlier Keve et al.[35] have also suggested absence of switching properties in $BaMnF_4$ compared to that in $BaZnF_4$, which is also in agreement with the present observed results. Thus it can be found that the decrease in distortion in the coordination polyhedra around the M^{2+} and Ba^{2+} ions has a strong influence on the ferroelectric properties. It can also be added here that the ionic polarizability does not have any predominant effect on the ferroelectric properties of $BaMF_4$ type compounds. This again indicates that the ferroelectricity in these

dx.doi.org/10.1021/ic201835q |*Inorg. Chem.* 2011, 50, 11765–11772

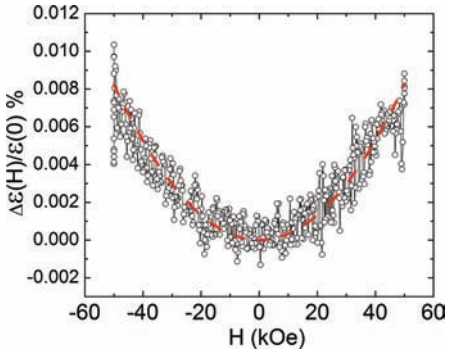

Figure 9. Magnetic field dependence of the capacitive response for different samples. The solid line is the fitted one.

systems is of different origin than in the conventional oxide perovskite ferroelectrics ($BaTiO_3$ or $PbTiO_3$) where charge transfer between the transition metal d and the oxygen's p orbital is crucial for stabilizing the noncentrosymmetric ferroelectric state.[34] It is quite unlikely that charge transfer from highly electronegative ion like fluoride to transition metal takes place in this system to stabilize the noncentrosymmetric ferroelectric state.

Thus an important finding of these studies is that as far as coexistence of ferroelectric and ferromagnetic properties is concerned, the 6 at % Mn substitution in $BaMgF_4$ exibits the best of both the properties.

3.6. Magnetocapacitance Behavior. The magnetic field dependence of capacitance for $BaMg_{1-x}Mn_xF_4$ samples has been measured. The representative room temperature magnetocapacitance for the $x = 0.06$ sample is shown in Figure 9. The capacitance data was noisy, as shown in Figure 9, where a dashed red line shows the theoretical fit to the functional form $\Delta\varepsilon(H)/\varepsilon(0) = \gamma H^2$, originating from the lowest order coupling terms polarization P and magnetization H in the free energy term.[36] These $BaMg_{1-x}Mn_xF_4$ ($0.0 \leq x \leq 0.15$) samples exhibit very weak magnetocapacitive coupling, which can be attributed to the very small magnetic signal observed in these samples. For the $x = 0.06$ sample, the magnetic field induced magnetocapacitive shift is ~0.008% in an applied field of 5 T. Such weak magnetocapacitance has been also observed in indium doped $YMnO_3$ multiferroic system.[36] The weak ferromagnetism in these systems is responsible for such low magnetocapacitance coupling in $BaMg_{1-x}Mn_xF_4$ ($0.0 \leq x \leq 0.15$) samples.

4. CONCLUSIONS

From the information set forth in this paper, it may be concluded that a new fluoride based series of materials with the general composition $BaMg_{1-x}Mn_xF_4$ ($0.0 \leq x \leq 0.15$) was synthesized by hydrothermal method. The room temperature ferromagnetism in $BaMgF_4$ could be induced by Mn^{2+} substitution. An optimum level of Mn^{2+} substitution is required to get the best of ferromagnetic and ferroelectric properties in these samples. Ferroelectricity is found to decrease with increase in Mn content in the series which is due to decrease in distortion. A very weak coupling behavior has been found which is attributed to the weak ferromagnetism present in the samples. These results will open various possibilities in view of the fact that for the first time a fluoride based material is shown to exhibit multiferroic properties. The first-principles spin-polarized calculations validated the effect of Mn substitution on the magnetic properties of $BaMgF_4$ and confirmed the decrease in magnetic moment with an increase in Mn content.

■ ASSOCIATED CONTENT

Supporting Information. (SI 1) XRD patterns of $BaMg_{1-x}Mn_xF_4$ ($x = 0.0, 0.08, 0.15$). (SI 2) SEM images of $BaMgF_4$ at different magnifications. (SI 3) Ratio of Ba:Mg:Mn in different compositions of $BaMg_{1-x}Mn_xF_4$ systems as per EDS data. The error was less than 0.5% for Ba, Mg, and Mn content. (SI 4) DR-UV spectra of pure $BaMgF_4$. The calculated band gap is 5.63 eV. This material is available free of charge via the Internet at http://pubs.acs.org.

■ AUTHOR INFORMATION

Corresponding Author

*Phone: 0091-22-2559 5330. Fax: 0091-22-25505151 E-mail: aktyagi@barc.gov.in.

■ ACKNOWLEDGMENT

The authors are thankful to Dr. S. N. Achary, BARC, for fruitful discussion.

■ REFERENCES

(1) Schmid, H. *Multiferroic Magnetoelectrics, Ferroelectrics* **1994**, *162*, 317.
(2) Wood, V. E.; Austin, A. E. *Magnetoelectronic Interaction Phenomena in Crystals*; Freemann, A. J.; Schmid, H., Eds. London: Gordon and Beach, 1975.
(3) Fiebig, M.; Lottermoser, T.; Frohlich, D.; Goltsev, A. V.; Pisarev, R. V. *Nature* **2002**, *419*, 818.
(4) Ascher, E.; Rieder, H.; Schmid, H.; Stossel, H. *J. Appl. Phys.* **1966**, *37*, 1404.
(5) Smolenskii, G. A.; Chupis, I. *Ferroelectromagnets, Sov. Phys. Usp.* **1982**, *25*, 475.
(6) Hill, N. A. *J. Phys. Chem. B* **2000**, *104*, 6694.
(7) Khomskii, D. I. *J. Magn. Magn. Mater.* **2006**, *306*, 1.
(8) Cheong, S. W.; Mostovoy, M. *Nat. Mater.* **2007**, *6*, 13.
(9) Neaton, J. B.; Ederer, C.; Waghmare, U. V.; Spaldin, N. A.; Rabe, K. M. *Phys. Rev. B* **2005**, *71*, 014113.
(10) Hill, N. A.; Rabe, K. M. *Phys. Rev. B* **1999**, *59*, 8759.
(11) Lottermoser, T.; Lonkai, T.; Amann, U.; Hohlwein, D.; Ihringer, J.; Fiebig, M. *Nature* **2004**, *430*, 541.
(12) Kimura, T.; Goto, T.; Shintani, H.; Ishizaka, K.; Arima, T.; Tokura, Y. *Nature* **2003**, *426*, 55.
(13) Fukumura, T.; Jin, Z; Kawasaki, M.; Shono, T.; Hasegawa, T.; Koshihara, S. *Appl. Phys. Lett.* **2001**, *78*, 958.
(14) Peleckis, G.; Wang, X. L.; Dou, S. X. *J. Magn. Magn. Mater.* **2006**, *301*, 308.
(15) Eibschütz, M.; Guggenheim, H. J.; Wemple, S. H.; Camlibel, I.; DiDomenico, M., Jr. *Phys. Lett. A* **1969**, *29*, 409.
(16) Shannon, R; D. *Acta Crystallographica A* **1976**, *32*, 751.
(17) Scott, J F *J. Phys.: Condens. Matter* **2008**, *20*, 021001.
(18) Pintilie, L; Alexe, M. *Appl. Phys. Lett.* **2005**, *87*, 112903.
(19) Dawber, M; Rabe, K. M.; Scott, J. F. *Rev. Mod. Phys.* **2005**, *77*, 1083.
(20) Scott, J. F. *J. Mater. Res.* **2007**, *22*, 2053.
(21) Catalan, G. *Appl. Phys. Lett.* **2006**, *88*, 102902.
(22) Catalan, G.; Scott, J. F. *Nature* **2007**, *448*, E4.
(23) Scott, J. F. *Ferroelectr. Rev.* **1998**, *1*, 1.
(24) Zhao, C.; Feng, S.; Xu, R.; Shi, C.; Ni, J. *Chem. Commun.* **1997**, 945.

(25) Estermann, M.; Mccusker, L. B.; Baerlocher, C.; Merrouche, A; Kessler, H. A. *Nature* **1991**, *352*, 320.
(26) Gingl, F. *Z. Anorg. Allg. Chem.* **1997**, *623*, 705.
(27) Aoki, A. *Japan J. App. Phys.* **1976**, *15*, 305.
(28) Carver, J. C.; Schweitzer, G. K.; Carson, T. A. *J. Chem. Phys.* **1972**, *57*, 973.
(29) Kumar, M. M.; Srinath, S.; Kumar, G. S.; Suryanarayana, S. V. *J. Magn. Magn. Mater.* **1998**, *188*, 203.
(30) Jaiswal, A.; Das, R.; Vivekanand, K.; Abraham, P. M.; Adyanthaya, S.; Poddar, P. *J. Phys. Chem. C* **2010**, *114*, 2108.
(31) Perdew, J. P.; Burke, K.; Wang, Y. *Phys. Rev.* **1996**, *B54*, 16533.
(32) Kresse, G.; Furthmüller, J. *Comput. Mat. Sc.* **1996**, *6*, 15.
(33) Blöchl, P. E. *Phys. Rev. B* **1994**, *50*, 17953. Kresse, G.; Joubert, J. *Phys. Rev. B* **1999**, *59*, 1758.
(34) Ederer, C.; Spaldin, N. A. *Phys Rev B* **2006**, *74*, 024102.
(35) Keve, E. T.; Abrahams, S. C.; Bernstein, J. L. *J. Chem. Phys.* **1969**, *51*, 4928.
(36) Dixit, A; Smith, A. E.; Subramanian, M. A.; Lawes, G. *Solid State Commun.* **2010**, *150*, 746.